



**HAL**  
open science

## Enzymatic activity monitoring through dynamic nuclear polarization in Earth magnetic field

E. Parzy, D. Boudries, Samuel Jacoutot, Muriel Albalat, Nicolas Vanthuyne, J-M Franconi, P. Mellet, E. Thiaudiere, G. Audran, S. R. A. Marque, et al.

### ► To cite this version:

E. Parzy, D. Boudries, Samuel Jacoutot, Muriel Albalat, Nicolas Vanthuyne, et al.. Enzymatic activity monitoring through dynamic nuclear polarization in Earth magnetic field. *Journal of Magnetic Resonance*, 2021, 333, pp.107095. 10.1016/J.Jmr.2021.107095 . hal-03516873

**HAL Id: hal-03516873**

**<https://hal.science/hal-03516873>**

Submitted on 7 Jan 2022

**HAL** is a multi-disciplinary open access archive for the deposit and dissemination of scientific research documents, whether they are published or not. The documents may come from teaching and research institutions in France or abroad, or from public or private research centers.

L'archive ouverte pluridisciplinaire **HAL**, est destinée au dépôt et à la diffusion de documents scientifiques de niveau recherche, publiés ou non, émanant des établissements d'enseignement et de recherche français ou étrangers, des laboratoires publics ou privés.



Distributed under a Creative Commons Attribution - NonCommercial - NoDerivatives 4.0 International License

# Enzymatic activity monitoring through dynamic nuclear polarization in Earth magnetic field

E. Parzy<sup>a,\*</sup>, D. Boudries<sup>a</sup>, Samuel Jacoutot<sup>b</sup>, Muriel Albalat<sup>c</sup>, Nicolas Vanthuyne<sup>c</sup>, J-M Franconi<sup>a</sup>, P. Mellet<sup>a,d</sup>, E. Thiaudiere<sup>a</sup>, G. Audran<sup>b</sup>, S.R.A. Marque<sup>b</sup>, P. Massot<sup>a</sup>

<sup>a</sup>Magnetic Resonance of Biological Systems, UMR5536 University of Bordeaux-CNRS, Bordeaux, France

<sup>b</sup>Aix Marseille Univ, CNRS, ICR, Case 551, 13397 Marseille, France

<sup>c</sup>Aix Marseille Univ, CNRS, ISM2, 13397 Marseille, France

<sup>d</sup>INSERM, Bordeaux

## A B S T R A C T

Cost-effective and portable MRI systems operating at Earth-field would be helpful in poorly accessible areas or in developing nations. Furthermore Earth-field MRI can provide new contrasts opening the way to the observation of pathologies at the biochemical level. However low-field MRI suffers from a dramatic lack in detection sensitivity even worsened for molecular imaging purposes where biochemical specificity requires detection of dilute compounds. In a preliminary spectroscopic approach, it is proposed here to detect protease-driven hydrolysis of a nitroxide probe thanks to electron-nucleus Overhauser enhancement in a home-made double resonance system in Earth-field. The combination of the Overhauser effect and the specific enzymatic modification of the probe provides a smart contrast reporting the enzymatic activity. The nitroxide probe is a six-line nitroxide which lines are shifted according to its substrate/product state, which requires quantum mechanical calculations to predict EPR line frequencies and Overhauser enhancements at Earth field. The NMR system is equipped with a 13-mT prepolarization coil, a 153-MHz EPR coil and a 2-kHz NMR coil. Either prepolarized NMR or DNP-NMR without prepolarization provide NMR spectra within 3 min. The frequency dependence of Overhauser enhancement was in agreement with theoretical calculations. Protease-mediated catalysis of the nitroxide probe could only be measured through the Overhauser effect with 5 min time resolution. Future developments shall open the way for the design of new low-field DNP-MRI systems.

## 1. Introduction

MRI has become one of the most prominent approach in medical imaging. It provides fine contrasts, decent resolution in three dimensions and presumable innocuousness at low or regular magnetic fields. However conventional MRI suffers from low sensitivity, lack of specificity at the molecular level and high purchase and operating costs. To palliate the sensitivity problem the trend is to use higher polarization fields, making the systems more expensive both in terms of manufacturing and maintenance. Such systems are affordable by major medical structures or research laboratories in wealthy countries. Moreover they are not moveable and cannot be brought in isolated areas thus excluding many pop-

ulation groups. Therefore alternate portable and cost-efficient MRI systems which would operate at low or very low fields are welcome. Since the pioneering work by Béné [1], such developments of low-field and/or portable MRI were explored for decades [2–5]. Low-field MRI provides additional advantages, such as better safety for patients with metallic implants, higher contrasts, radiation penetration depth and safety. An obvious low-field drawback is the dramatic loss of sensitivity that prompted to develop various strategies in order to compensate for.

The first way to improve sensitivity is to temporarily increase the magnetic field before application of an MRI sequence of acquisition [1,4,6]. However, situations where the signal level may remain weak requires additional developments. For instance, the use of SQUID (Superconducting Quantum Interference Device) alleviates the problem by reducing noise and provides gain sensitivity [7,8]. Other approaches use magnetization transfer from hyperpolarized species like noble gas [9,10] or solid-state dynamic nuclear polarization before dissolution and transfer to a nuclei of interest

\* Corresponding author at: Centre de Résonance Magnétique des Systèmes Biologique, UMR5536, Case 93 Université de Bordeaux-CNRS, 146, rue Léo Saignat, F-33076, France.

E-mail address: [elodie.parzy@u-bordeaux.fr](mailto:elodie.parzy@u-bordeaux.fr) (E. Parzy).

[11], or even parahydrogen-induced polarization [12] with a spin order transfer from nascent protons to  $^{13}\text{C}$  or  $^{15}\text{N}$ . The advantage of the latter techniques is that increased sensitivity can be combined with biochemical specificity for molecular imaging. Thereby, enzymatic reactions have been demonstrated *in vivo* [13,14] in mice at high fields. Albeit very attractive the use of transiently hyperpolarized species are not suitable for long-term *in situ* metabolic observations e.g. for hours. However, on-demand signal enhancement can be produced through another phenomenon, Dynamic Nuclear Polarization by Overhauser effect [15]. In an PEDRI (Proton-Electron Double Resonance Imaging) or Overhauser-MRI (OMRI) experiment [16,17], Zeeman states of unpaired electrons of a radical are saturated through continuous-wave electron spin resonance experiment resulting in a polarization transfer to the proton spins in their vicinity. For *in vivo* molecular imaging, OMRI can be used to detect an enzymatic activity provided the EPR signature of a free-radical substrate changes upon catalytic conversion into the reaction product. This principle was successfully used to detect the activity of a protease, namely neutrophil elastase *in vitro* [18] and *in vivo* pancreatic elastase in mouse intestine [19] at 0.19 T. In parallel a new kind of nitroxides [20] for which EPR lines can be shifted upon hydrolysis were developed to monitor neutrophil elastase activity [21]. Very interestingly, by changing EPR frequency either the nitroxide substrate (an enol-ester) or its product (a ketone) can be selectively imaged, making possible the use of such elastase-specific nitroxides for monitoring *in vivo* up-regulated neutrophil elastase that can be found in a variety of inflammatory diseases. An example of the OMRI-detection of a line-shifting nitroxide in mice with inflamed lungs at 0.19 T was recently published [22]. Such a tool would be invaluable to characterize such diseases in the future, as well as for novel anti-protease testing. Unfortunately OMRI as a molecular imaging technique cannot be used *in vivo* at high magnetic field because EPR requires irradiation at microwave frequencies (around GHz or higher) with shallow wave penetration and unacceptable heating. *In vivo* experiments were nevertheless possible at 0.19 T in small animals but much lower field (<1 mT) are mandatory to apply OMRI *in vivo* on larger animals, let alone on humans. Importantly, it has been shown theoretically and then experimentally that the DNP enhancement factor increases with decreasing static magnetic field [23,24] when radical species with hyperfine splitting are used. In the area of molecular MRI, such an effect can be used to partially counterbalance the loss of NMR signal at very low fields.

In this preliminary work, it is proposed to use DNP in Earth field to detect the time-course of human neutrophil elastase activity

*in vitro*. Both the reactant (Fig. 1A) and the reaction product (Fig. 1B) are nitroxides which display hyperfine coupling with both  $^{14}\text{N}$  and  $^{31}\text{P}$ , resulting in 6 EPR lines at high field<sup>20,21</sup>. In a first step, theoretical calculations were carried out in order to predict EPR lines and Overhauser enhancements as a function of magnetic field. In a second step Overhauser effects were measured *in vitro* in the local earth field on the reaction product at *ca.* 150 MHz EPR frequency. Finally kinetics of elastase-driven nitroxide hydrolysis was measured.

## 2. Theory and calculations

In the nitroxides used here, the electronic spin ( $S=1/2$ ) interacts with the nuclear  $^{14}\text{N}$  spin ( $K=1$ ) and the  $^{31}\text{P}$  spin ( $P=1/2$ ) of the same molecule through hyperfine coupling. To calculate the maximum DNP factor (DNPF) and frequencies associated, the simplified Hamiltonian matrix is first defined to give access to the energy levels of the system.

As it is not possible to calculate the matrix of spin relaxation for an unknown number of magnetic nuclei in one molecule, we consider the simple case of interaction between one electron spin and one  $^{14}\text{N}$  and one  $^{31}\text{P}$  spin. Nitroxide-nitroxide interaction (diluted case) was neglected in an isotropic medium in a constant magnetic field  $B_0$  aligned along the z-axis.

The Hamiltonian can be written as (in angular frequency unit):

$$\begin{aligned} \widehat{H}_0 = & \omega_e \widehat{S}_z + \omega_N \widehat{K}_z + \omega_P \widehat{P}_z + a_N \left[ \widehat{S}_z \widehat{K}_z + \frac{1}{2} (\widehat{S}_+ \widehat{K}_- + \widehat{S}_- \widehat{K}_+) \right] \\ & + a_P \left[ \widehat{S}_z \widehat{P}_z + \frac{1}{2} (\widehat{S}_+ \widehat{P}_- + \widehat{S}_- \widehat{P}_+) \right] \end{aligned} \quad (1)$$

where  $a_N$  and  $a_P$  are the isotropic hyperfine constants,  $\omega_e$ ,  $\omega_N$ ,  $\omega_P$ , are the electron and nuclear Zeeman frequencies, and  $\widehat{S}_i$ ,  $\widehat{K}_i$  and  $\widehat{P}_i$  the electron, nitrogen and phosphorus nuclear spin operators with  $i = z, +$  or  $-$ .

As the magnetic field decreases, the hyperfine interactions predominate more and more over the Zeeman effect. Consequently, the stationary Hamiltonian, although Hermitian, is no longer diagonal. The Hamiltonian corresponds to a  $12 \times 12$  matrix and which is as such not analytically diagonalizable. In such an SKP system, the energy levels correspond to the eigen-states  $|F, m_F\rangle$  where  $F = \widehat{S} + \widehat{K} + \widehat{P}$  is the total spin and  $m_F = m_s + m_K + m_P$  its z-component. The eigen-energies and wave functions were numerically calculated with Python 2 software. Calculations included the following experimental values for the coupling constants pre-

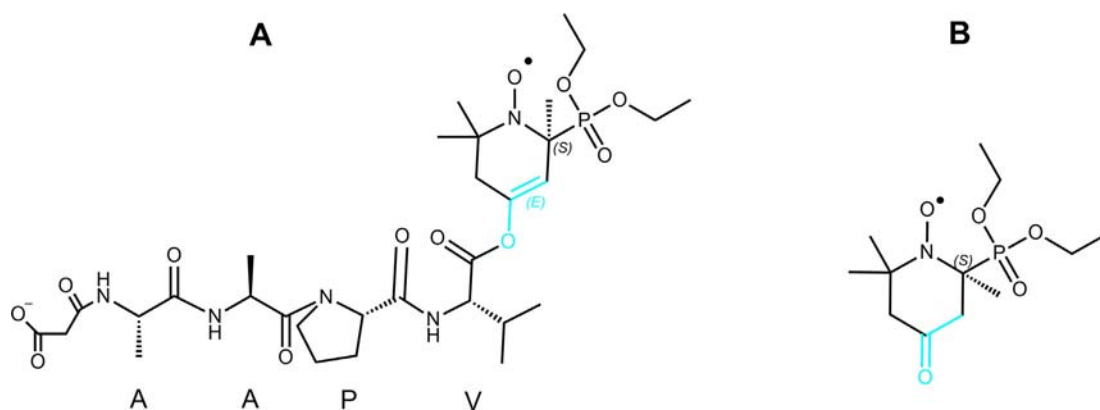


**Fig. 1.** (A) Neutrophil elastase nitroxide substrate. The nitroxide was esterified as an enol ester of the peptide Suc-Ala-Ala-Pro-Val. (B) Reaction product (ketone form). The enol-ester and ketone function are highlighted in cyan. (For interpretation of the references to colour in this figure legend, the reader is referred to the web version of this article.)

viously determined by X-band EPR [21]:  $a_N = 1.5\text{mT}$  and  $a_P = 3.84\text{mT}$  for the substrate, and  $a_N = 1.49\text{mT}$  and  $a_P = 4.33\text{mT}$  for the product.

The EPR transition is achieved with a continuous electromagnetic wave of  $B_2$  amplitude at an angle  $\theta$  from  $B_0$ . The corresponding Hamiltonian is given as :

$$\hat{H}_{\text{irradiation}} = -\gamma_e B_2 (\cos \theta \hat{S}_z + \sin \theta \hat{S}_x) \quad (2)$$

with  $\gamma_e$ , the electron gyromagnetic ratio. A  $\pi$ -transition corresponds to  $\theta = \pi/2$  whereas a  $\sigma$ -transition is excited at  $\theta = 0$ . Only  $\pi$ -transitions will be considered below. They correspond to the selection rule  $\Delta m_F = +1$  if left circularly polarized  $B_2$  wave is used or  $\Delta m_F = -1$  with left circularly polarized waves. The transition probabilities between states  $|i\rangle$  and  $|j\rangle$  are then calculated according to the equation:

$$W_{ij} = C \langle i | (\hat{S}_+ - \hat{S}_-) | j \rangle \quad (3)$$

where C is a normalization constant.

The energy levels dependence as a function of static magnetic field are depicted in Fig. 2. A total of 14  $\pi$ -transitions and 6  $\sigma$ -transitions were calculated.

The calculation of the dynamic nuclear polarization factor (DNPF) was carried out as already described by Guiberteau and Grucker for a 3-line nitroxide [23]. It is defined as:

$$\text{DNPF} = \varepsilon - 1 = \rho f s \left[ \frac{\langle S_z \rangle - S_0}{I_0} \right] \quad \text{with} \quad \varepsilon = \frac{\langle I_z \rangle}{I_0} \quad (4)$$

$$\langle S_z \rangle - S_0 = \sum_i \langle i | S_z | i \rangle (n_i - n_i^0)$$

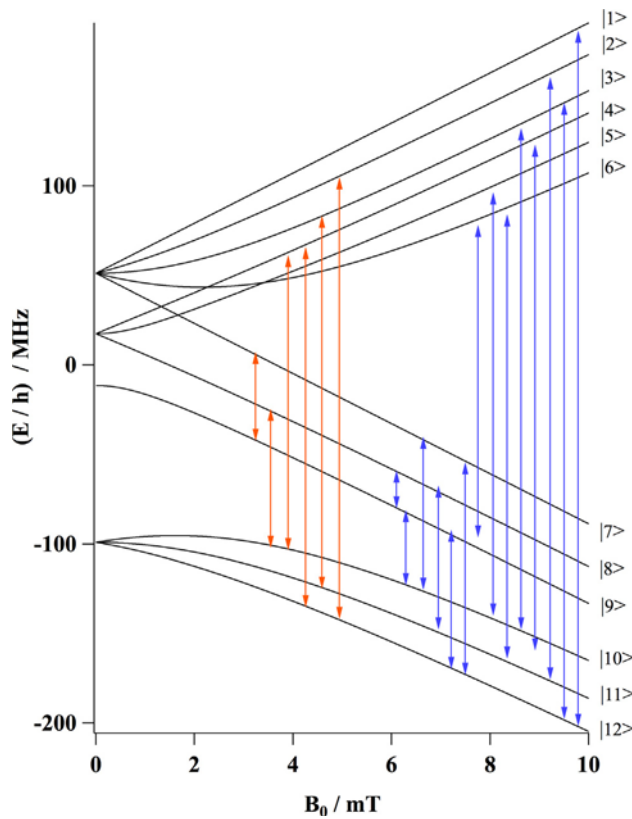


**Fig. 2.** Electron energy levels (divided by Planck's constant) as function of the external magnetic field for a 3 spins system: unpaired electron spin,  $^{14}\text{N}$  and  $^{31}\text{P}$  nucleus spins of the ketone product. Blue double-head arrows:  $\pi$ -transitions; orange double-head arrows:  $\sigma$ -transitions. (For interpretation of the references to colour in this figure legend, the reader is referred to the web version of this article.)

Here,  $\varepsilon$  is the enhancement factor,  $\rho$  is the electron-nucleus coupling factor,  $f$  the leakage factor,  $s$  the saturation ratio, and  $n_i$  and  $n_i^0$ , the population of the  $i$ -state respectively without and with the saturation of the transition.

At thermal equilibrium and under high-temperature approximation, the population of the  $i$ -state is calculated as :

$$n_i^0 = \frac{1}{(2S+1)(2K+1)(2P+1)} \left( 1 - \frac{E_i}{kT} \right) \quad (5)$$

Considering the same assumptions as Guiberteau and Grucker [23]:

$$n_i = n_j = \frac{n_i^0 + n_j^0}{2}, \quad \forall i \neq j \quad (6)$$

$$\Delta n_k = 0, \quad \forall k \neq i,$$

the expression of a DNP factor for the saturation of each EPR transition (DNPF<sub>ij</sub>) can be written as:

$$\text{DNPF}_{ij} = \frac{\rho f s}{n \gamma_i B_0} (E_i - E_j) (\langle i | S_z | i \rangle - \langle j | S_z | j \rangle) \cdot W_{ij} \quad (7)$$

with  $\gamma_i$  the gyromagnetic ratio of the proton and  $n = (2S+1)(2K+1)(2P+1)$ ,  $n = 12$  in the present case. Fig. 3 shows the maximum DNPF for the substrate Suc-(Ala) 2-Pro-Val-enol-ester (green) and the ketone product (red) at 43.9  $\mu\text{T}$ . To calculate this parameter, the saturation is assumed to be perfect ( $s = 1$ ), without Heisenberg electron spin exchange as the nitroxide is very diluted [25]. The proton longitudinal relaxation was assumed to be only due to the presence of the electron spin ( $f = 1$ ) and a pure dipolar coupling was considered ( $\rho = 0.5$ ). Of note, the occurrence of both positive and negative DNPF is the consequence of  $\Delta m_F = -1$  and  $\Delta m_F = +1$ , respectively.

As shown in Fig. 3 the higher DNPF were found at around 140 MHz for the substrate or around 150 MHz for the product with three positive and three negative lines. These frequencies correspond to roughly  $1.5(a_N + a_P/2)$ , expressed in frequency unit, similarly to what was observed with three-line nitroxides [23] where  $a_P = 0$ . In a DNP experiment using a single EPR frequency, the frequency shift occurring in the substrate-to-product conversion is large enough to provide a clear disambiguation between them. A similar effect was already observed at high field [21].

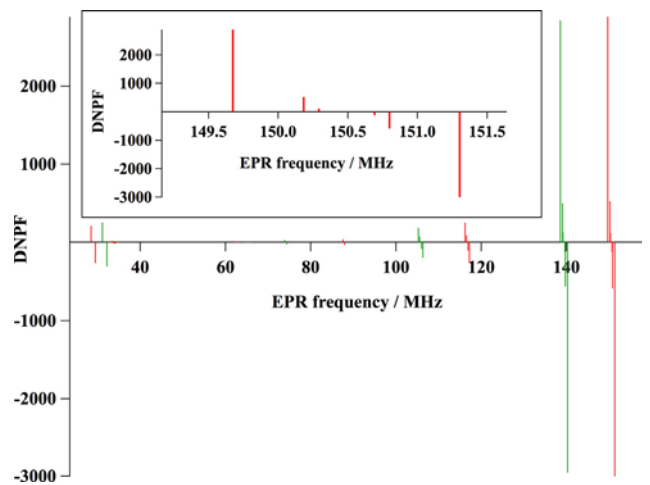


**Fig. 3.** Simulated maximum DNP enhancement factors relative to  $\pi$  transitions electron frequencies at 43.9  $\mu\text{T}$  with  $s = 1$ ,  $f = 1$  and  $\rho = 0.5$ . Hyperfine coupling constants :  $a_N = 1.5\text{mT}$  and  $a_P = 3.84\text{mT}$  for the substrate (in green), and  $a_N = 1.49\text{mT}$  and  $a_P = 4.33\text{mT}$  for the product (in red)<sup>21</sup>. Insert : expanded 150 MHz-spectral region for the ketone product. (For interpretation of the references to colour in this figure legend, the reader is referred to the web version of this article.)

### 3. Materials and methods

#### 3.1. Chemicals

Neutrophil Elastase was purchased from Elastin Products Company (Missouri, USA). Suc-Ala-Ala-Pro-Val-Nitroxide and ketone-Nitroxide (both diastereoisomer *S*) were synthesized and purified as already described [21]. DNP experiment was carried out with Suc-Ala-Ala-Pro-Val-Nitroxide (1.2 mM) in a 30-mL vial in HEPES buffer 50 mM at pH 7.4, 0.15 M NaCl and 0.05% Igepal (Sigma-Aldrich, St. Quentin Fallavier, France). The proteolysis reaction was started with the addition of 40 nM neutrophil elastase.

#### 3.2. Earth-Field DNP setup

All experiments were performed with a home-built Earth-field NMR spectrometer, working at 1.9 kHz in the local field of the laboratory ( $\sim 43.9\mu\text{T}$ , Fig. 4). The setup was derived from Carl Michal's experimental setup [26] and used the spectrometer software environment developed under free software license (GNU-GPL, version 3), called ANMR application. Basically this equipment was used with or without magnetic prepolarization at 13 mT, and makes possible Dynamic Nuclear Polarization through Electron Spin Resonance at Earth field. Some adjustments were necessary to establish the communication protocols between the NMR application software written under Python 2.7 on a Windows 7© (Microsoft Corp. Redmond, WN, U.S.) platform and the Arduino Integrated Development Environment software coded in C language (arduino.cc). All the hardware control and the signal sampling is done within the Arduino Uno embedded software platform in controller's integrated Analog-Digital Converter (ATmega328 microcontroller, Atmel, San Jose, CA).

Details on the hardware elements are given below.

#### 3.3. Prepolarization coil

The home-made solenoid coil was made as previously described by Michal. The inner diameter was 160 mm, allowing the integration of the other parts of the system. The solenoid was made of 3-layer windings connected in parallel giving an equivalent inductance of *ca.* 610  $\mu\text{H}$  supporting a total direct current of 18 A under 11 V at 13 mT. The switch from 0 to 13 mT induction was achieved adiabatically within 60 ms. Commutation delays were controlled via the software interface and the sequence programs.

#### 3.4. NMR transmit-receive coil

The NMR coil consisted in a 12-layer solenoid wound up on a domestic 50 mm-diameter PVC tube. Solenoid length was 75 mm, the inner duty diameter was 45 mm. A total number of 3146 turns of 0.25 mm-diameter enameled copper wire were wound up. Each coil layer was separated by additional insulating tape to reduce the stray capacitance of the coil. The measured coil resistance was 192 Ohms, estimated inductance in the order of 294mH, and the coil self-resonance frequency, due to the stray capacitance has been measured at 13 kHz, well above the NMR frequency. This coil was tuned to the receiver channel by a 27nF capacitor mounted in parallel to the first preamplifier stage input. The main axis of the NMR coil was oriented perpendicularly to the local Earth-field.

#### 3.5. EPR transmit coil

A saddle-shaped transmit coil (inner diameter: 31 mm; length: 45 mm) was designed (Igor Pro, Wavemetrics, Lake Oswego, OR) to operate at  $152 \pm 6$  MHz with a linear polarization. This coil was positioned colinearly within the NMR coil. Coil tuning and matching were carried out at the coil's end with a classical variable capacitor circuit, using fixed non-magnetic capacitors ATC (ATC

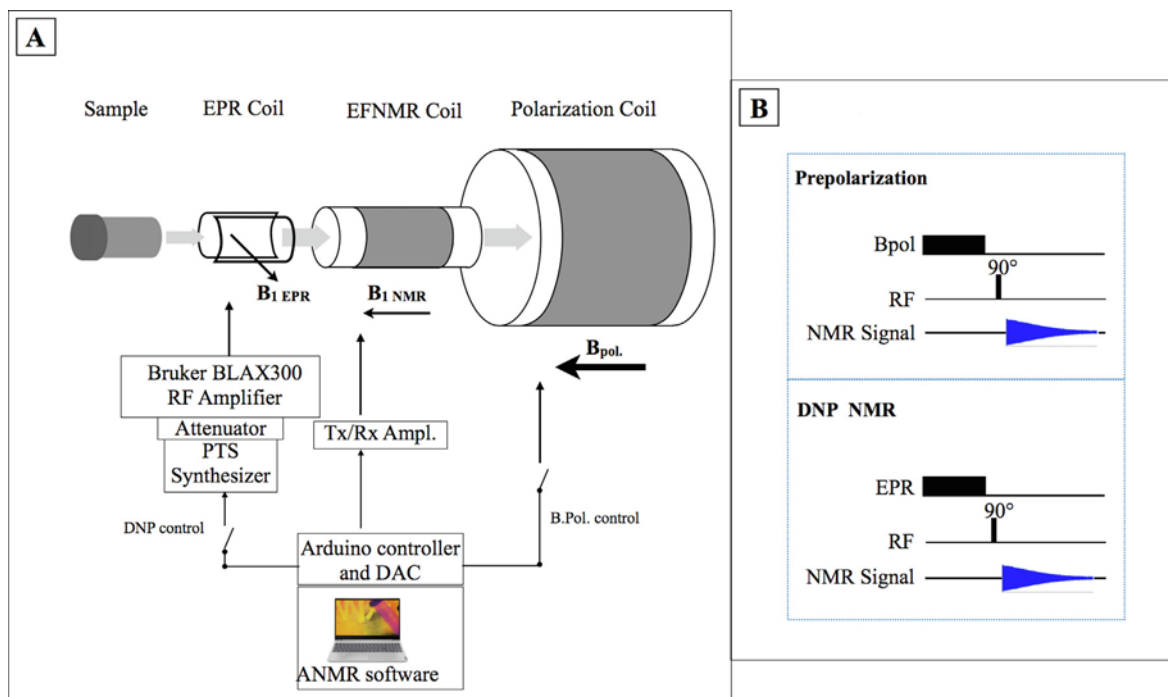


**Fig. 4.** Earth-field DNP setup and pulse sequence timing. (A). The Arduino controller was used to selectively activate either the DNP acquisition with the EPR coil (DNP control) or the prepolarization step at 13 mT (B. pol. control). The radiofrequency fields were orthogonal to Earth field. Vertical arrows stand for control over EPR emission (left), NMR transmit-receive coil (middle) and prepolarization coil (right). Other arrows indicate the orientation of the electromagnetic (EPR or NMR) and prepolarization field. (B) Pulse sequences used for prepolarized or DNP-enhanced NMR with a  $90^\circ$  nutation angle for proton excitation (RF).

American Technical Ceramics, NY 11746), and non-magnetic variable (0.8 to 18pF) capacitors (Polyflon company, Norwalk, CT 06,851 USA). The coil and tuning circuit supports was made on a 3D printer "Form 3" and resins from Formlabs Inc., Somerville, MA 02143, USA. Owing to the EPR coil geometry, with the EPR  $B_2$  field perpendicular to the main coil axis it was possible to rotate it inside the NMR coil so as to position the  $B_2$  field either perpendicular or parallel to the Earth magnetic field, or in any intermediate angle position. In the present study,  $B_2$  was kept orthogonal to the Earth-field in order to select EPR  $\pi$ -transitions.

### 3.6. EPR RF channel

This RF channel was made with refurbished NMR hardware and was able to generate RF pulses from 1 MHz to 160 MHz. Pulse durations and associated delays were controlled via the ANMR software. The RF wave was generated by a PTS-160 Synthesizer (Programmed Test Source Inc., Littleton, MA) with a modified manual frequency control box (Siemens AG, Erlangen, Germany). The minimal frequency step was 10 Hz, while PTS resolution was 1 Hz, and a manual step attenuator, 0–63 dB, 1 dB step (RLC Electronics, New-York, USA) was used. The frequency/phase and amplitude stability of this PTS synthesizer, used originally in a MRI system was much greater than needed here. This controlled frequency signal was fed through a BLAX300 300 W power amplifier (Bruker Biospin SA, Wissembourg, France). The logical ON/OFF pulse command issued from the Arduino board was done via an optical link to ensure electrical insulation (omitted for simplicity in Fig. 4). This command was sent to a locally build optical/electrical, battery supplied, interface connected to the "Unblank" input of the amplifier and controls the power output. The attenuator inserted between the PTS output and the power amplifier allowed to control the EPR power in 1 dB steps. Since we used very long EPR RF pulses, up to 500 ms, it may be considered as continuous wave mode for the amplifier, and in this case power was limited to 30 W (amplifier specification). For the sake of safety a maximum of 15 W power was preferred, corresponding to an actual deposited power at the sample level of 5–6 W, as estimated from temperature elevation (data not shown).

### 3.7. Pulse sequences and acquisition protocols

The original ANMR setup functionalities were used here. The "Pulse-FID" sequence timing was adapted to the DNP application. In particular, delays required for solenoid coils switching (in case of magnetic prepolarization, due to current discharging time and oscillation problems linked to coil coupling with co-linear magnetic fields), were eliminated in the DNP experiment. Thus, the sum of the delays between preparation step (prepolarization) and EFNMR experiment was not the same for each experiment. In case of magnetic prepolarization, this cumulated delay was 140 ms (including receiver delay) giving a recovery time (TR) of 954 ms and an acquisition time of 191 s (200 averages). For the DNP experiments, cumulated delays were reduced to 62 ms, allowing a TR of 876 ms, the overall acquisition time was 176 s (200 averages).

In DNP experiments, EPR was achieved with continuous irradiation for 500 ms at the electron frequency. Then a  $90^\circ$  RF-pulse (2.15 ms) was applied at 1868 Hz for proton resonance at 43.9  $\mu$ T before FID signal recording (3000 data points, dwell-time : 100  $\mu$ s). The minimum delay between the EPR CW and the NMR pulse was 62 ms.

To estimate the DNP enhancement as a function of EPR irradiation frequency, 22 spectra were acquired at different EPR frequencies ranging from 146 to 157 MHz. The sample used was a 30-mL vial with 1.2 mM ketone-nitroxide

As no signal could obviously be recorded at local Earth-field within 176 s (see Fig. 5C), prepolarized NMR acquisition was conducted as a reference signal. In such experiment, the prepolarization at 13 mT was applied for 500 ms.

The DNP enhancement factor was calculated as follows:

$$\varepsilon = \frac{S_{DNP} B_{POL}}{S_{POL} B_{EF}} \quad (8)$$

where  $S_{DNP}$  is the integrated NMR signal with DNP but without prepolarization,  $S_{POL}$  is the integrated NMR signal without DNP but with prepolarization  $B_{POL}$  is the prepolarization field (13 mT) and  $B_{EF}$  the local Earth magnetic field (43.9  $\mu$ T).

For kinetic measurements, the vessel of 30 ml was filled with 1.2 mM of Suc-(Ala) 2-Pro-Val nitroxide in HEPES. A first control DNP-NMR spectrum was acquired before the introduction of neutrophil elastase. Then, 15 DNP spectra were acquired every 5 min to follow the catalysis of proteolysis at an EPR frequency of 153 MHz.

## 4. Results

Fig. 5 A, B and C display proton Earth-field NMR spectra of the ketone sample (1.2 mM in water) recorded in the presence of prepolarization at 13 mT without EPR, in the presence of EPR at 153 MHz without prepolarization and in the absence of both, respectively. No significant signal was recorded at Earth-field under conventional NMR acquisition (Fig. 5C), as expected because of the very low polarization of proton spin at 43.9  $\mu$ T (0.15 ppb).

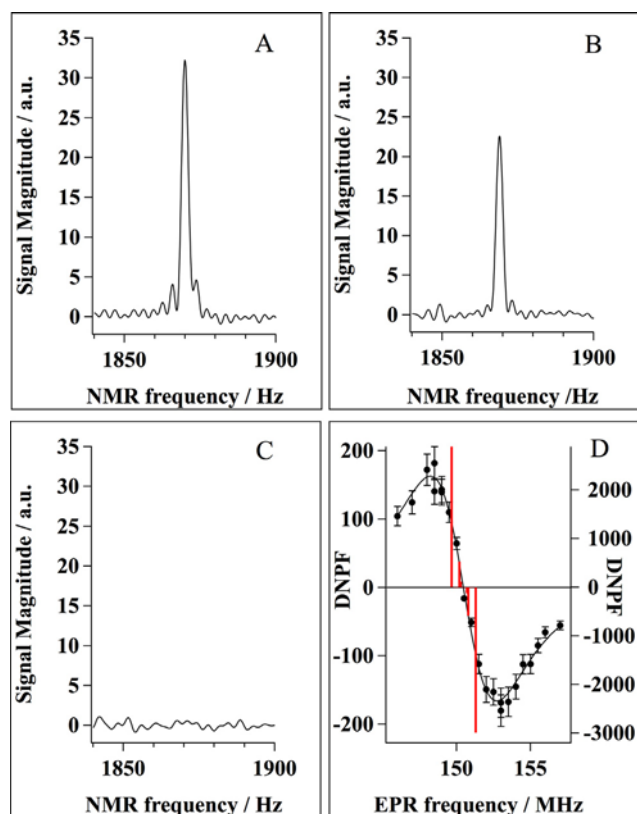


Fig. 5. Earth-field NMR acquisition. (A,B,C). Proton NMR spectra of 1.2 mM ketone nitroxide in water in the presence of prepolarization at 13 mT, in the presence of EPR at 153 MHz or in the absence of both, respectively. (D) Frequency dependence of the measured Overhauser effect (left axis). The curve fit (solid line) corresponds to Eq. (7) with  $f = 0.51$ ,  $\rho = 0.36$  and  $s = 0.5$  and line positions (rad bars, right axis) of the theoretical spectrum displayed in the insert of Fig. 3. The linewidth corresponds to an electron T2-value of 43 ns.

Conversely, a measurable signal was observed with 200 averaged scans, either under prepolarization or EPR irradiation at 153 MHz. The latter frequency corresponded to  $\pi$ -transitions of the unpaired electron of the 6-line nitroxide (Fig. 3). The marked increase in the NMR signal under EPR irradiation can obviously be attributed to the Overhauser effect. Without DNP, the presence of the nitroxide would not have been detected by conventional NMR, albeit in Earth-field or prepolarized. Only the application of DNP can reveal either the decrease of substrate that is hydrolysed by the enzyme or the formation of the new nitroxide, product of this reaction. Signal-to-noise ratios under DNP or prepolarization conditions were in the range of 10 and the linewidth was in the range of 5 Hz. Assuming  $T_1 = T_2 = 3$  s in the extreme narrowing limit, the observed linewidth corresponded to an averaged spatio-temporal field inhomogeneity of about 1300 ppm, an acceptable value considering that the experimental setup was housed in a regular university building. In order to confirm the theoretical calculation of the EPR spectrum of the nitroxide DNP experiments were carried out by varying the EPR frequency from 146 to 157 MHz. This frequency range was chosen because the DNPF at other frequencies were expected much lower (Fig. 3). Moreover, the exploration of the Overhauser effect over the entire EPR frequency range would have required the manufacturing of many EPR coils.

The NMR peak area displayed a minimum at 153 MHz and a maximum at 149 MHz (Fig. 5D). Of note, phase-sensitive detection allowed a clear disambiguation of the positive and the negative enhancements. When compared with the theoretical spectrum (red bars in Fig. 5D) the measured position of the EPR lines as well as the poor observed resolution are due to fast electron transverse relaxation.

The observed Overhauser enhancements can be calculated from prepolarized and DNP spectra with Eq (8), and compared with the theoretical values, taking into account the  $T_2$  of electron. Experimental results were curve-fit with a multi-Lorentzian function, where the peak positions were fixed according to the theoretical calculation and the linewidth was an adjustable parameter. The goodness of fit was fairly acceptable and the transverse electron relaxation time was estimated to  $43 \pm 5$  ns. Because of large EPR linewidth (ca. 7 MHz), field inhomogeneity was negligible. Experimental enhancements at 153 MHz were around  $\pm 180$ , lower than the theoretical value of 2800/-3000 with  $f.s = 1$  and  $\rho = 0.5$  (pure dipolar coupling, see Eq(7)). The discrepancy can be accounted for by the inherently broad EPR lines due to the short electron  $T_2$  (estimated to 43 ns) which induced signal decrease from the overlap of proximate negative and positive lines. Moreover the coupling factor was likely lower than 0.5 (it was estimated as 0.36 from the results of Jugniot et al [21]) and the leakage factor was around 0.5 assuming a nitroxide relaxivity of  $0.4 \text{ s}^{-1}\text{mM}^{-1}$  (actually measured at 0.19 T) and a  $T_1$  value for free water of around 3 s. Based upon those parameters the actual saturation factor was calculated at 0.5, because of short EPR irradiation times (0.5 s) with respect to the  $T_1$  of water proton.

Overhauser enhancements provided by millimolar concentration of the ketone nitroxide were utilized to monitor the protease-mediated hydrolysis of the enol-ester nitroxide substrate (Fig. 1A). As seen from Fig. 3, EPR frequencies used for the ketone product (ca. 150 MHz) were ineffective to saturate the unpaired electron of the enol-ester substrate. Therefore the observation of DNP with a EPR frequency of 153 MHz allowed for the detection of the ketone product only, irrespective of the presence of the substrate. Therefore, the observed Overhauser enhancements were considered as high enough so that the DNP-NMR setup at Earth-field could be used to monitor the protease-mediated hydrolysis of the elastase nitroxide substrate by measuring the Overhauser effect of the ketone product. Thanks to the EPR line-shift operated

through the substrate-to-product conversion, no substrate observation was allowed by fixing the EPR frequency at 153 MHz at Earth-field, as expected from the calculation results in Fig. 3 and as seen from the first data of Fig. 6 at  $t = 0$  (before the addition of the enzyme). An example of kinetic measurement of ketone formation from 1 mM enol ester in the presence of 40 nM neutrophil elastase is depicted in Fig. 6. Overhauser-enhanced proton spectra monotonically increased reaching a plateau, indicating full conversion into the reaction product. The reaction half-time was roughly estimated to 50 min. Interestingly, an enzyme-catalyzed reaction, relevant to inflammatory diseases, could be assessed through the use of Earth-field Overhauser-enhanced NMR with a dedicated chemical contrast agent.

## 5. Discussion

The present work is at the crossroad of two different promising areas of research : i) the pursuit of « smart » chemical agents that make possible the spatial-temporal imaging of a biochemical activity *in vivo*, especially in the context of person-driven medicine ; ii) the future offer of low-field cost-efficient versatile MRI systems operating at low fields. In the latter case, a variety of solutions are under investigation to alleviate the dramatic loss of NMR signal at very low fields, e.g. hyperpolarization or superconducting detectors, each of them attractive as such. Here, it was chosen to use the « ready-to-use » earth-field in combination with an « in situ and on-demand » approach that might provide an NMR signal triggered by an enzyme. In a first step, a proof-of-concept was evaluated, where Overhauser-enhanced NMR spectroscopy was used to detect a protease-specific nitroxide.

The occurrence of two electron-nucleus hyperfine couplings, generating six EPR line at high field required quantum mechanical calculation that used the spin operator formalism to predict the EPR spectrum and Overhauser enhancement at low-field. As a result, the enol-ester nitroxide and the ketone nitroxide were predicted to display strongly shifted spectra owing to the difference in the electron-phosphorus hyperfine coupling constant. Such an effect was previously used at 0.19 T in Overhauser-enhanced MRI to assess the presence of either nitroxide at a given EPR microwave frequency. At very low fields the higher enhancements were predicted to arise at ca. 150 (140) MHz for the ketone (enol-ester). Such frequencies are compatible with EPR irradiation *in vivo*, an important issue when dealing with energy deposition. The calculated DNP-enhancement spectra bear both positive and negative lines, separated by a few hundreds of kHz. Due to the natural EPR linewidth (several MHz), the actual negative and positives

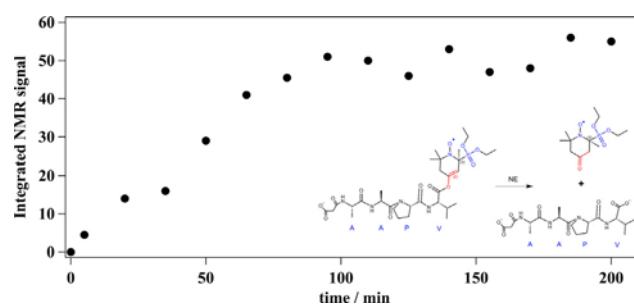


**Fig. 6.** Kinetics of neutrophil elastase (NE)-mediated proteolysis reaction of Suc-(Ala)<sub>2</sub>-Pro-Val-nitroxide enol ester into the ketone form observed through Earth-field Overhauser-enhanced NMR. The enol ester and ketone functional groups are indicated in red in the chemical structures. The substrate (1.2 mM) was mixed with the enzyme (40 nM) at  $t = 0$  and DNP-NMR was performed with an EPR frequency of 153 MHz at 15-minute intervals starting at  $t = 5$  min. (For interpretation of the references to colour in this figure legend, the reader is referred to the web version of this article.)

lines are mostly superimposed. When using linearly polarized waves for EPR saturation, contributions from both negative and positive lines to the Overhauser effect coexist and decrease the DNP. The reciprocal partial cancellation of opposite lines could be alleviated by the use of circularly polarized waves which can select one line polarity or the other.

In order to ascertain the feasibility of DNP-NMR at Earth-field using the predicted EPR frequencies, a complete setup was assembled. It gathered a prepolarization coil, an EPR and a NMR coil, two RF transmitter lines and one RF receiver line synchronized by an Arduino controller. Such a system is inherently flexible and cost-effective. It permitted NMR measurements within minutes even though the local field was poorly homogeneous. Obviously higher signal-to-noise ratio is expected in the case of better homogeneity, would it be 100 ppm. In future work, shim coils would be implemented for this purpose.

The measured frequency dependence of Overhauser enhancement, *i.e.* the shape of the DNP spectrum of the ketone nitroxide was in close agreement with the calculated data. The striking point was the occurrence of both positive and negative enhancements, which in some way validated the theoretical approach. Importantly, linearly polarized waves were used, which impeded the ability to select either positive or negative lines. Such a selection that can be achieved with circularly polarized light would provide higher enhancements by removing opposite overlapping lines in the DNP spectrum, as already reported [27]. In a preliminary work using circularly polarized waves (not shown) such an effect was indeed measured, but more work is needed for a better reproducibility.

The observed magnitude of the DNP enhancement compared well with the theoretical values. Here the nitroxide concentration was in the range of 1 mM, providing a leakage factor of about 0.5, assuming a  $T_1$ -value of free water of 3 s and a relaxivity value of the nitroxide of  $0.4 \text{ s}^{-1}\text{mM}^{-1}$ . Moreover, only 500 ms EPR time was used here, preventing complete electron saturation. The latter point might be improved in future MRI experiments, where EPR can be used continuously throughout a fast imaging acquisition for several seconds [19].

The EPR coil used here produced a highly homogeneous RF field. The RF power used for electron saturation was in the range of 5–6 W and corresponded to an average SAR of 50 W/kg or a temperature elevation of  $0.7 \text{ }^\circ\text{C}/\text{min}$  in water (neglecting heat transfer) if the DNP acquisition (200 scans, 3 min) is repeated every 5 min. In future *in vivo* experiments, lower SAR would be provided with circularly polarized RF coils and lower duty cycles.

The study focused on the ketone product using EPR at *ca* 150 MHz. Much work would have been required in order to evaluate in a similar approach the properties of the substrate at *ca* 140 MHz, namely the design and optimization of a new EPR coil.

The application of Overhauser-enhanced NMR to measure the catalysis of a nitroxide substrate at Earth-field was successful. The very high enhancements helped to acquire data in the minute time scale, which is well consistent with proteolysis time constants that can occur in living systems.

As a conclusion, it was shown here that Earth-field DNP experiments with a homemade system could be used to unveil a biological activity using dedicated nitroxides which EPR spectra can be theoretically predicted. One may emphasize that proteolysis of nitroxide substrate could not be observed in Earth-field without DNP. Technical improvements are obviously needed in order to gain sensitivity and decrease the SAR, especially in future MRI applications. For instance the use of circularly polarized EPR irradiation is expected to provide three to four times higher Overhauser enhancements in Earth's field as compared to linearly polarized EPR waves. In parallel the use of new nitroxides exhibiting narrower EPR lines would help to ensure a better electron saturation

in DNP experiments. As for NMR detection the use of gradiometers would allow higher signal-to-noise ratio. Work is in progress in order to upgrade the present setup into a MRI system that would allow the tracking of proteolysis in preclinical studies on rodents. Prepolarized MRI would provide anatomical images whereas DNP would highlight the enzymatic activity at similar space-resolutions, given the high DNPs observed in the millimolar range. Since the nitroxides used here are well tolerated by rodents [21,22] their use in drug-testing protocols *in vivo*, *e.g.* protease inhibitors, would be of great help in anti-inflammation therapy evaluation for instance in the context of chronic Obstructive Pulmonary Disease or cystic fibrosis.

- [1] G.J. Béné, Nuclear magnetism of liquid systems in the earth field range, *Phys. Rep. Rev. Sec. Phys. Lett.* 58 (4) (1980) 213–267, [https://doi.org/10.1016/0370-1573\(80\)90012-5](https://doi.org/10.1016/0370-1573(80)90012-5).
- [2] Stepišnik J., Eržen. V., Kos M. NMR imaging in the earth's magnetic field. *Magn Reson. Med.*, 15:3 (1990) 386–91. 10.1002/mrm.1910150305
- [3] Mohoric A., Stepišnik J., Kos M., Planinšič G. Self-diffusion imaging by spin echo in Earth's magnetic field, *J. Magn. Reson.*, 136:1 (1999) 22–6. 10.1006/jmre.1998.1594
- [4] M.E. Halse, A. Coy, R. Dykstra, C. Eccles, M. Hunter, R. Ward, P.T. Callaghan, A practical and flexible implementation of 3D MRI in the Earth's magnetic field, *J. Magn. Reson.* 182 (1) (2006) 75–83, <https://doi.org/10.1016/j.jmr.2006.06.011>.
- [5] Wald L.L., McDaniel P.C., Witzel T., Stockmann J.P., Cooley C.Z. Low-cost and portable MRI. *J Magn Reson Imaging.* 2020 Sep;52(3) (2020) 686–696. 10.1002/jmri.26942
- [6] Mohoric A., Planinšič G., Kos M., Duh A., Stepišnik J. Magnetic resonance imaging system based on Earth's magnetic field. *Instrum. Sci. Technol.*, 32 (2004), 655–67. 10.1081/CI-200037034
- [7] McDermott R., Trabesinger A.H., Mück M., Hahn E.L., Pines A., Clarke J. Liquid-State NMR and Scalar Couplings in Microtesla Magnetic Fields. *Science* 295 (2002) 2247–49. 10.1126/science.10692805
- [8] McDermott R., Lee S.K., ten Haken B., Trabesinger A. H., Pines A., Clarke J. Microtesla MRI with a superconducting quantum interference device. *Proc. Nat. Acad. Sci.* 101:21 (2004)7857–61. 10.1073/pnas.0402382101
- [9] Colegrove, F.D., Scheerer, L.D., and Walters, G.K. (1963). Polarization of He3 Gas by Optical Pumping. *Phys. Rev.* 132 (1963) 2561–2572. 10.1103/PhysRev.132.2561

- [10] T.G. Walker, W. Happer, Spin-exchange optical pumping of noble-gas nuclei, *Rev. Mod. Phys.* 69 (1997) 629–642, <https://doi.org/10.1103/RevModPhys.69.629>.
- [11] Ardenkjær-Larsen J.H., Fridlund B., Gram A., Hansson G., Hansson L., Lerche M. H., Servin R., Thaning M., Golman K. Increase in signal-to-noise ratio of >10,000 times in liquid-state NMR. *Proc. Nat. Acad. Sci.* 100:18 (2003) 10158–63. [10.1073/pnas.1733835100](https://doi.org/10.1073/pnas.1733835100)
- [12] C.R. Bowers, D.P. Weitekamp, Transformation of Symmetrization Order to Nuclear-Spin Magnetization by Chemical Reaction and Nuclear Magnetic Resonance, *Phys. Rev. Lett.* 57 (1986) 2645–2648, <https://doi.org/10.1103/PhysRevLett.57.2645>.
- [13] P. Dzien, M.I. Kettunen, I. Marco-Rius, E.M. Serrao, T.B. Rodrigues, T.J. Larkin, K. N. Timm, K.M. Brindle, <sup>13</sup>C magnetic resonance spectroscopic imaging of hyperpolarized [1-<sup>13</sup>C, U-<sup>2</sup>H<sub>5</sub>] ethanol oxidation can be used to assess aldehyde dehydrogenase activity in vivo, *Magn. Reson. Med.* 73 (5) (2015) 1733–1740, <https://doi.org/10.1002/mrm.25286>.
- [14] N.M. Zacharias, H.R. Chan, N. Sailasuta, B.D. Ross, P. Bhattacharya, Real-time molecular imaging of tricarboxylic acid cycle metabolism in vivo by hyperpolarized 1-<sup>13</sup>C diethyl succinate, *J. Am. Chem. Soc.* 134 (2) (2012) 934–943, <https://doi.org/10.1021/ja2040865>.
- [15] A. Abragam, M. Goldman, Principles of dynamic nuclear polarisation, *Rep. Prog. Phys.* 41 (3) (1978) 395.
- [16] D. Lurie, J.M.S. Hutchison, L.H. Bell, I. Nicholson, D.M. Bussell, J.R. Mallard, Field-cycled proton–electron double-resonance imaging of free radicals in large aqueous samples, *Magn. Reson.* 84 (1989) 431–437, [https://doi.org/10.1016/0022-2364\(89\)90392-2](https://doi.org/10.1016/0022-2364(89)90392-2).
- [17] D. Grucker, In Vivo Detection of Injected Free Radicals by Overhauser Effect Imaging, *Magn. Reson. Med.* 14 (1990) 140–147, <https://doi.org/10.1002/mrm.1910140113>.
- [18] E. Parzy, V. Bouchaud, P. Massot, P. Voisin, N. Koonjoo, D. Moncelet, J.M. Franconi, E. Thiaudière, P. Mellet, Overhauser-enhanced MRI of elastase activity from in vitro human neutrophil degranulation, *PLoS One* 8 (2) (2013), <https://doi.org/10.1371/journal.pone.0057946> e57946.
- [19] N. Koonjoo, E. Parzy, P. Massot, M. Lepetit-Coiffé, S.R. Marque, J.M. Franconi, E. Thiaudière, P. Mellet, In vivo Overhauser-enhanced MRI of proteolytic activity, *Contrast Media Mol Imaging* 9 (5) (2014) 363–371, <https://doi.org/10.1002/cmimi.1586>.
- [20] Audran G., Bosco L., Brémond P., Franconi J.M., Koonjoo N., Marque S.R., Massot P., Mellet P., Parzy E., Thiaudière E. Enzymatically Shifting Nitroxides for EPR Spectroscopy and Overhauser-Enhanced Magnetic Resonance Imaging. *Angew Chem Int Ed Engl.* 54:45 13379–84. [10.1002/anie.201506267](https://doi.org/10.1002/anie.201506267)
- [21] N. Jugniot, I. Dutttagupta, A. Rivot, P. Massot, C. Cardiet, A. Pizzoccaro, M. Jean, N. Vanthuyne, J.M. Franconi, P. Voisin, G. Devouassoux, E. Parzy, E. Thiaudière, S.R.A. Marque, A. Bentaher, G. Audran, P. Mellet, An elastase activity reporter for Electronic Paramagnetic Resonance (EPR) and Overhauser-enhanced Magnetic Resonance Imaging (OMRI) as a line-shifting nitroxide, *Free Radic. Biol. Med.* 126 (2018) 101–112, <https://doi.org/10.1016/j.freeradbiomed.2018.08.006>.
- [22] Rivot A., Jugniot N., Jacoutot S., Vanthuyne N., Massot, P., Mellet P., Marque S.R. A, Audran G., Voisin P., Delles M., Devouassoux G., Thiaudière E., Bentaher A., Parzy E. Magnetic Resonance Imaging of Protease-Mediated Lung Tissue Inflammation and Injury. *ACS Omega* 6:23 (2021) 15012–15016. [10.1021/acsomega.1c01150](https://doi.org/10.1021/acsomega.1c01150)
- [23] T. Guibertau, D. Grucker, Dynamic nuclear polarization at very low magnetic fields, *Phys. Med. Biol.* 43 (7) (1998) 1887–1892, <https://doi.org/10.1088/0031-9155/43/7/009>.
- [24] M.E. Halse, P.T. Callaghan, A dynamic nuclear polarization strategy for multi-dimensional Earth's field NMR spectroscopy, *J. Magn. Reson.* 195 (2) (2008) 162–168, <https://doi.org/10.1016/j.jmr.2008.09.007>.
- [25] Lingwood M.D. , Ivanov I.A. , Cote A.R. , Han S. Heisenberg spin exchange effects of nitroxide radicals on Overhauser dynamic nuclear polarization in the low field limit at 1.5 mT *J. Magn. Reson.* 204 (2010) 56–63. [10.1016/j.jmr.2010.01.015](https://doi.org/10.1016/j.jmr.2010.01.015)
- [26] C.A. Michal, A low-cost spectrometer for NMR measurements in the Earth's magnetic field, *Meas. Sci. Technol.* 21 (2010), <https://doi.org/10.1088/0957-0233/21/10/105902> - [10.1088/0957-0233/21/10/105902](https://doi.org/10.1088/0957-0233/21/10/105902) 105902.
- [27] Hilschenz I., Oh S., Lee S.J., Kyu Yua K., Hwang S. , Kim K., Hyun Shim J. Dynamic nuclear polarisation of liquids at one microtesla using circularly polarised RF with application to millimetre resolution MRI. *J. Magn Reson* 305 (2019) 138–45 [10.1016/j.jmr.2019.06.013](https://doi.org/10.1016/j.jmr.2019.06.013)